

# Elemental fractionation of dielectric aerosols produced by near-infrared femtosecond laser ablation of silicate glasses†

J. Koch,\* H. Lindner, A. von Bohlen, R. Hergenröder and K. Niemax

ISAS—Institute for Analytical Sciences, Bunsen-Kirchhoff-Strasse 11, D-44139 Dortmund, Germany. E-mail: koch@ansci.de; Fax: +49-231-1392-120; Tel: +49-231-1392-175

Received 2nd March 2005, Accepted 3rd June 2005

First published as an Advance Article on the web 1st July 2005

The composition and fractionation properties of dielectric aerosols generated by near-infrared femtosecond laser ablation of silicate glass (carrier gas: helium, 1 atm) have been examined. Aerosols were classified using low-pressure impaction of particles with diameters from 7 nm up to 7  $\mu\text{m}$ . The element-selective analyses of impacted material has been restricted to minor matrix constituents (nominal concentration  $\sim 4.5\%$ ) applying total reflection X-ray fluorescence. It has been found that for fluences larger than 5  $\text{J cm}^{-2}$  the total Zn-, Ca-, Sr-, Ba-, and Pb-specific composition of these aerosols corresponds to that of the bulk material even though the size-dependent particle composition strongly altered. Typical deviations were of the order of 5–10%. In contrast, fluences below 5  $\text{J cm}^{-2}$  usually resulted in stronger differences from the bulk composition indicating intensified fractionation during the ablation process. Our results furthermore demonstrate, that the major fraction of the aerosol mass is located within the mesoscopic size range, *i.e.* from 10 up to 100 nm, fairly independent on the fluence applied. However, the relative percentage of micrometer particles has been found to significantly decrease for higher fluences. Scanning electron microscopy of impacted brass particles moreover revealed a fractal-like structure of deposits. Implications for the classification of such structures using low-pressure impaction are discussed.

## Introduction

Laser ablation inductively-coupled plasma mass spectrometry (LA-ICP-MS) is being considered as one of the most versatile methods for the element-selective analysis of solid material due to its sensitivity and conceptual simplicity. Ever since the first feasibility studies carried out during the 1980s<sup>1,2</sup> the performance characteristics of LA-ICP-MS have constantly been enhanced. For instance, various laser wavelengths, carrier gases, and cell designs have been examined to specify optimum conditions for improving the efficiency and accuracy of analysis.<sup>3–5</sup> Moreover, great effort has been made for the development of different calibration strategies to further increase the flexibility.<sup>6,7</sup> As a result, LA-ICP-MS using UV-type laser sources has been brought up to a powerful method, in particular, with respect to the non-matrix-matched analysis of silicate glasses and minerals.<sup>8,9</sup> Nevertheless, LA-ICP-MS is still far from being completely accepted as a universal method due to the persistent deficiency of adequate reference materials leading to non-accurate quantification due to elemental fractionation. In order to achieve an optimum performance of analysis, evaporated sample material (i) should reflect the exact bulk composition, (ii) is converted into an aerosol that can efficiently be transported to the detector site, and (iii) must completely be decomposed within the ICP source. The examination of these effects represents a crucial issue due to their obvious complexity involving laser-, transport-, and ICP-, *i.e.* plasma-induced phenomena. Among these, the investigation of laser-induced effects is of particular interest as it pre-defines transport- and plasma-induced fractionation.

As pointed out earlier (see, *e.g.* ref. 10) laser-induced fractionation results from the thermal character of nanosecond LA, involving processes such as preferential evaporation and heat penetration into the target due to thermal diffusion, which

hold the risk of material re-distribution and cumulative enrichment of certain constituents. Furthermore, strong energy dissipation within the expanding material as a result of plasma shielding may intensify “non-stoichiometric” etching of the target surface particularly at the edges of the exposed area. In addition, material ejection partly overlaps with the pulse duration implying that vapour and particulate matter (grown as well as splashed particles) undergo persistent laser interaction, which might also affect the aerosol formation or composition.

In order to eliminate or at least efficiently suppress such collateral effects the pulse duration has to be chosen to be sufficiently small compared to the material-specific thermal relaxation time of the electronic subsystem. According to Chichkov *et al.*<sup>11</sup> these are of the order of a few picoseconds, depending on the material considered. In fact, the application of pulse durations below these time constants has been proven favourable for the analysis of solid matter concerning the suppression of elemental fractionation. For instance, Russo *et al.*<sup>12</sup> found fractionation during the analysis of silicate glasses by near-IR (NIR) femtosecond (fs) LA-ICP-MS to be minor if the sampling process is accomplished in the low fluence regime ( $\sim 3 \text{ J cm}^{-2}$ ). In contrast, Bian *et al.*<sup>13</sup> recently demonstrated accurate, non-matrix matched analyses of various brass, Al, and silicate glass standards applying NIR-fs-LA-ICP optical emission spectrometry (OES) at higher fluences ( $> 5 \text{ J cm}^{-2}$ ).

However, the direct quantification of laser-produced aerosols by ICP spectrometry provides only information about the overall fractionation which is blamed to be system-dependent thus giving no insight into laser-induced processes. Therefore, the composition of primary aerosols has lately been studied.<sup>14</sup> It could be shown that NIR-fs-LA of brass using moderate fluences ( $< 5 \text{ J cm}^{-2}$ ) enables the production of ultra-fine, nearly stoichiometric aerosols. For non-conducting, *i.e.* dielectric matter, however, these conditions certainly depart from those specified since such materials only provide a minor number of free electrons that can directly couple to the incident

† Presented at the 2005 European Winter Conference on Plasma Spectrochemistry, January 30–February 3, 2005, Budapest, Hungary.

laser radiation and are moreover characterized by a comparatively high evaporation enthalpy. Therefore, the fluence range for “stoichiometric” or “congruent” ablation is supposed to be different, in particular, if UV-transparent materials such as fused silica, MgF<sub>2</sub>, CaF<sub>2</sub>, or LiF<sub>2</sub> are under investigation.

The present article reports on laser-induced fractionation of dielectric aerosols produced by NIR-fs-LA of multi-component silicate glasses. According to investigations previously published<sup>14</sup> the aerosols were classified using low-pressure impaction of particles covering a size range from about 7 nm up to 7 μm. After classification the collected material was Zn-, Ca-, Sr-, Ba-, and Pb-specifically analysed by TXRF. To specify conditions advantageous for the suppression of laser-induced fractionation, analyses were carried out for varying fluences, ranging from threshold-close values of 1 up to 20 J cm<sup>-2</sup>.

## Experimental

A sketch of the experimental arrangement used for aerosol production and classification is shown in Fig. 1. Femtosecond pulses (pulse duration 100 fs, center wavelength 795 nm) were generated by a CPA-type Ti : Sa laser system (Hurricane, Spectra Physics, Mountain View, CA, USA). The radiation was delivered to a plano-convex lens ( $f = 100$  mm) using a set of dielectric mirrors and subsequently focused onto the surface of a glass sample (multi-component glass, NIST 1412) positioned in the centre of a cylindrical, Al-made ablation cell ( $V_{\text{cell}} = 15$  cm<sup>3</sup>, inlay material: Teflon<sup>®</sup>). The lateral sample position was adjusted from outside using a pair of micrometer screws, both integrated in the bottom of the ablation cell. Therefore, the relative positions of laser spot and ablation cell remained unchanged throughout sampling. In order to keep particle losses due to diffusion and electrostatic settling during transportation as small as possible, the ablation cell and outlet connection piece were grounded and directly attached to the inlet stage of the impactor unit. A series of 25 craters with a diameter of about 50 μm was shot each run. For better comparison, the laser repetition rate and exposure time per spot were set to conditions previously chosen for the investigations on brass, *i.e.* 10 Hz and 32 s, respectively. Helium was chosen as the carrier gas.

The spot size of the laser beam at the sample surface was estimated *via* crater diameters or damage radii, respectively evaluated for ascending pulse energies assuming the beam profile to be gaussian-type. As a result, energy densities specified in the present article refer to peak fluences instead of mean values. A complete description of this procedure can be found, for instance, in ref. 15.

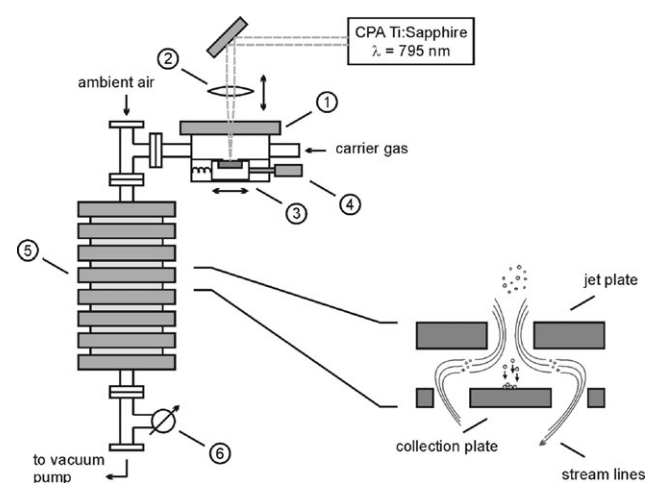


**Fig. 1** Experimental arrangement used for the classification of laser-produced glass aerosols. Working principle of low-pressure impaction: (1) ablation cell, (2) focussing lens ( $f = 100$  mm), (3) movable sample holder, (4) micrometer screw, (5) impactor stage, (6) pressure gauge.

## Classification and low-pressure impaction of particles

Aerosols were classified using a 13-stage, low-pressure impactor (DLPI, Dekati<sup>®</sup>, Tampere, Finland) which is designed for the collection of airborne particles ranging from 10 nm up to 10 μm aerodynamic diameter. Taking into account a particle density of the NIST standard used ( $\sim 3$  g cm<sup>-3</sup>) this range corresponds to about  $7 \text{ nm} \leq d_p \leq 7 \text{ μm}$  physical or so-called Stokes diameter. Detailed information on operational and general performance characteristics of the impactor used can be found in ref. 16. The composition of the glass standard used can be extracted from Table 1. Please note that the constituents specified refer to those elements which can be measured by TXRF with sufficient sensitivity.

The particles were deposited on flat PMMA discs (diameter 26 mm, thickness 3 mm), which were inserted into special home-made collection plates. The outer dimensions of these plates were exactly adapted to the design of the original ones. In order to prevent bounce- and blow-off effects during classification the central part of the PMMA discs was pre-treated using a minor quantity of pure Vaseline<sup>®</sup>.

## TXRF analysis

After classification, the collected material was Zn-, Ca-, Sr-, Ba-, and Pb-specifically analysed by total reflection X-ray fluorescence spectrometry. For this purpose, an amount of about 10 μL Ge-containing alkaline solution—corresponding to 1–5 ng Ge absolute—was applied to each PMMA disc as internal standard and evaporated by infrared radiation. Element-specific analyses were subsequently performed using a commercial TXRF instrument (EXTRA II, R. Seifert & Co, Ahrensberg, Germany) equipped with a Si(Li) detector/analyser system (QX 2000, Link System, Oxford Instruments, High Wycombe, UK). Masses were calculated directly from relative line intensities taking into account the response of the internal standard used. The deposits were irradiated by a Mo X-ray tube applying a voltage of 50 kV at a maximum current of 38 mA. Depending on the quantity of material to be analysed an acquisition time between 100 and 300 s was chosen. Experimental uncertainties were of the order of 5–10% relative which, however, drastically increased up to 40% when working close to the detection limit.

## Results and discussion

### Accuracy of low-pressure impaction

The application of low-pressure impaction enables the classification of particles according to their so-called relaxation time  $T$  which is defined by the product of mass and mobility. In a few words,  $T$  represents the duration a particle needs to be redirected to the streamlines after being accelerated through the jet plate nozzle. Obviously, particles with  $T_{\text{upper}} \leq T \leq T_{\text{lower}}$  settle down on the same stage independent of their individual size or shape. Considering, for instance, fluffy or fractal-like structures the relaxation time of single particles and agglomerates can nearly remain constant provided that the

**Table 1** Ca-, Zn-, Sr-, Ba-, and Pb-specific composition of the NIST 1412 silicate glass standard and corresponding weight ratios relative to Zn

Constituent <sup>b</sup>	Percent by weight <sup>b</sup>	Element/Zn weight ratio/g g <sup>-1</sup>
Ca	4.53	0.90
Zn <sup>a</sup>	4.48	1.00
Sr	4.55	1.07
Ba	4.67	1.16
Pb	4.40	1.14

<sup>a</sup> Internal standard. <sup>b</sup> Refers to the element oxide.

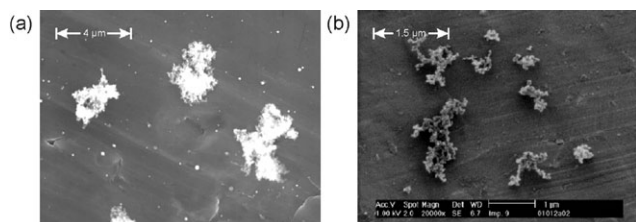


**Fig. 2** Comparison of the fractal-like structure of laser-produced brass (a) and soot particles (b), by courtesy of C. Van Gulijk (Delft University of Technology, Netherlands).

particle size distribution of the primary aerosol is sufficiently narrow and the fractal dimension  $d_f$  is less than two.<sup>17</sup> Furthermore, agglomerates formed should be smaller than the molecular mean free path which is usually fulfilled under conditions prevalent during low-pressure impaction. In the late 1980s, it has already been shown that such fractal structures are formed, for instance, during continuous wave (CW) LA of solid matter or the combustion process of diesel fuels resulting in the emission of soot particles.<sup>18,19</sup> In fact, the morphology of deposits studied in the present work is quite similar to these particles implying that particles produced by NIR-fs-LA and corresponding agglomerates may, in principle, be deposited on the same stage if the rules of fractal particle growth apply and  $d_f \leq 2$ . In Fig. 2 the fractal-like structure of soot and laser-produced particles is depicted.†

To prove the accuracy of classification during impaction, particles from laser-produced brass aerosols deposited on different stages were examined *via* high-resolution scanning electron microscopy (SEM; instrument: H-S4500 FEG, Hitachi High Technology Europe GmbH, Krefeld, Germany). The particles were collected on clean aluminium substrates. In Fig. 3 and 4, SEM micrographs of deposits taken from the impactor stages 4, 6, and 9—corresponding to mean particle sizes of 38 nm, 120 nm, and 620 nm, respectively—are shown as examples. Apparently, the major part of the material collected on stage 4 consists of agglomerates composed of primary particles whose size complies with the diameter range specified for this particular stage. It is, however, questionable whether these agglomerates were exclusively formed during the ablation process and transport period since their overall size ranges up to about 5 μm. Most intuitively, clustering or stacking of smaller agglomerates and single particles right before impaction in front of the collection plate appears to be the most reasonable mechanism for creating such structures. Nevertheless, the above-mentioned concept of corresponding relaxation times theoretically permits the deposition of such large agglomerates on stages which are designed for the collection of nanoparticles or small clusters only. It is interesting to note that the deposits shown in Fig. 4 obviously form a self-affinity pattern rather than a uniform one, *i.e.* both agglomeration and deposition of agglomerates during impaction seem to follow the same rules of fractal growth. In Fig. 4(a) and (c), the self-affinity of laser-produced deposits is illustrated by comparing the complete micrograph with a substructure blown up to the same size.

In contrast, particles which were deposited on stages 6 and 9 were found to match to the expected size range, *i.e.* in between  $90 \leq d_p \leq 160$  nm and  $480 \leq d_p \leq 800$  nm (see Fig. 3).

† The fractal dimension  $d_f$  of agglomerates refers to their average density, *i.e.* the smaller the  $d_f$  the less dense the agglomerate. Here, a dimension of 3 indicates the limiting case of a solid sphere. Assuming the agglomerate to be composed of almost mono-disperse aerosol particles  $d_f$  is therefore correlated to the surface area which is exposed to the ambient. As a consequence, the fractal dimension may be regarded as an indicator for the dissociation capability of agglomerates when penetrating a plasma source that is operated at a given temperature. Methods to determine  $d_f$  are discussed, for instance, in ref. 17.

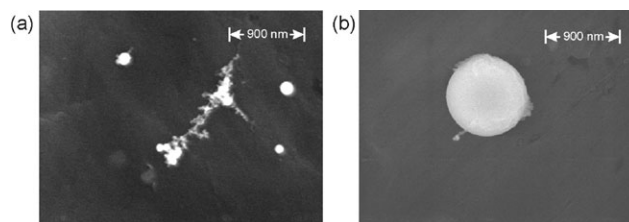


**Fig. 3** SEM micrographs of brass deposits taken from the impactor stages 6 and 9—corresponding to mean particle sizes of 120 nm (a) and 620 nm (b), respectively.

However, it has also been observed that the impaction of micrometer particles is usually accompanied by the deposition of smaller, nano-sized structures as a result of diffusional settling. According to the manufacturer corresponding losses should be smaller than 5% even for particles whose diameter is of the order of 10 nm. Consequently, these deposits cannot significantly contribute to the total mass collected on this stage. In extreme cases (mono-disperse aerosols with  $d_p \ll 10$  nm), however, material loss due to diffusional settling might alter the aerosol composition (totally and size-dependent) or shift the real particle size distribution towards larger particle diameters.

#### Mass and number distributions

In Fig. 5 a mass distribution of an aerosol produced by NIR-fs-LA of glass at a fluence of  $9.5 \text{ J cm}^{-2}$  using He as carrier gas is shown. Please note that the data depicted correspond to the cumulative Ca-, Zn-, Sr-, Ba-, and Pb-specific values. Apparently, the aerosol mainly consists of particles within the mesoscopic size range, *i.e.* roughly in between 10 and 100 nm. The corresponding number distribution which was calculated assuming a spherical particle shape has been found to be shifted down by 85 nm towards a mean diameter to about 15 nm. Furthermore, the width of the number size distribution (FWHM criterion) shown in Fig. 6 has been determined as less than about 25 nm. It is evident that such aerosols can be treated as nearly mono-disperse therefore meeting the above-mentioned requirement of fractal clustering or particle growth, respectively. Both mean diameter and width have been derived taking into account a log-normal fitting function. The assumption of log-normal distributions has *no* theoretical basis yet but has been found to be applicable to most aerosols originating from a single source.<sup>20</sup> However, efforts to explain the log-

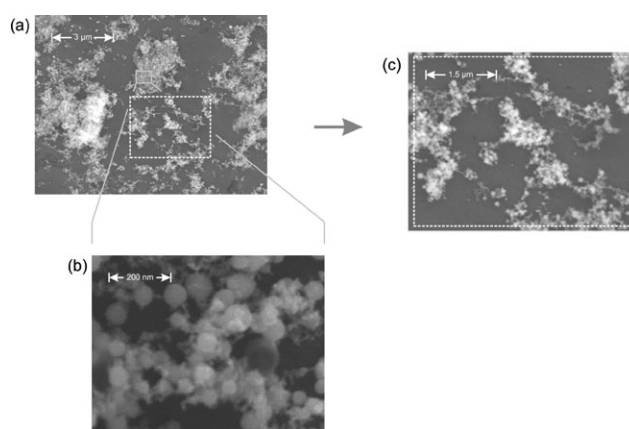


**Fig. 4** SEM micrographs of brass deposits taken from impactor stage 4—corresponding to a mean particle size of 38 nm (see (a) and (b)). In (a) and (c), the self-affinity of laser-produced deposits is illustrated by comparing the complete micrograph with a substructure blown up to the same size (dashed rectangle). Please note that the structure shown in (b) was scanned separately and represents *no* digital magnification of the cut-out.

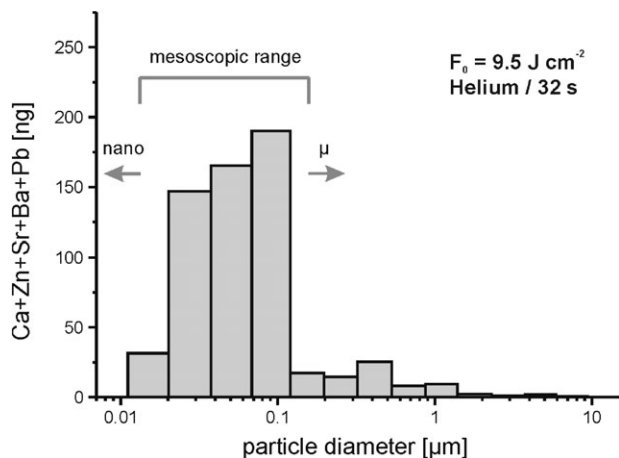


**Fig. 5** Typical mass distribution of an aerosol produced by NIR-fs-LA of glass at  $9.5 \text{ J cm}^{-2}$  using He as carrier gas. The masses given refer to cumulative Ca-, Zn-, Sr-, Ba-, and Pb-specific values.

normal nature of measured particle size distributions from first principles in a physically realistic way are presently being made.<sup>21</sup>

It should be re-emphasized that the data given in Fig. 5 refer to a certain fraction of the total mass deposited since the analysis has been restricted to the quantification of Zn, Ca, Sr, Ba, and Pb only. However, a comprehensive analysis of the deposits should result in similar size distributions as long as condensation from supersaturated vapour can be assumed to be the dominant mechanism of particle growth. In order to demonstrate the conformance of individual, *i.e.* elemental and cumulative mass distributions, in Fig. 7, the Zn- and (Ca + Sr + Pb + Ba)-specific data are compared as examples.

Although most of the aerosol mass ablated was found to settle down within stages covering the mesoscopic size range it has been observed that there always exists a certain fraction of micrometer particles, as can be seen from Fig. 5. Those particles, however, cannot be grown from supersaturated vapour due to an extremely high cooling rate of the expanding material which is of the order of  $10^{10}$ – $10^{11} \text{ K s}^{-1}$ .<sup>22</sup> Mechanisms potentially relevant for the formation of such particles are, for instance, splashing or hydrodynamic instabilities. From an analytical point of view, the production of  $\mu\text{m}$ -sized particles is known to reinforce elemental fractionation as a result of incomplete evaporation within the ICP source, as indicated by Kuhn *et al.*<sup>23</sup> In Fig. 8, the relative percentage of particles, *i.e.* aerosol mass, beyond a diameter of  $0.5 \mu\text{m}$  is plotted *versus* the fluence applied. Apparently, the total mass of

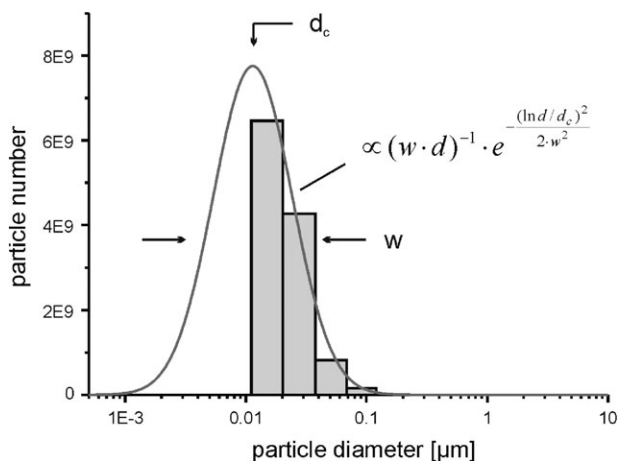


**Fig. 6** Number distribution based on the data shown in Fig. 5. Values were determined assuming a spherical particle shape. The regression (grey curve) was performed using a log-normal fitting function.

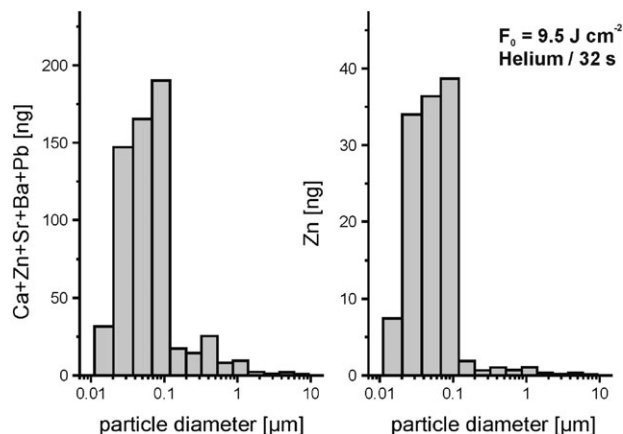


**Fig. 7** Comparison of the individual Zn- and cumulative (Ca + Sr + Pb + Ba)-specific mass distributions for NIR-fs-LA of silicate glass at a fluence  $9.5 \text{ J cm}^{-2}$ .

particles  $> 0.5 \mu\text{m}$  reaches a maximum value of nearly 20% at  $2 \text{ J cm}^{-2}$  which, however, drops below 5% for fluences greater than  $10 \text{ J cm}^{-2}$ .

### Elemental fractionation

As already suggested above, the examination of laser-induced fractionation represents a key issue for developing strategies that enable the accuracy of LA-ICP spectrometry to be increased to the maximum extend possible. In order to specify conditions favourable for the production of stoichiometric glass aerosols, in the present work, the deviation of the elemental mass ratio  $\delta M_{\text{element}}$  has been determined using Zn as internal reference. By definition  $\delta M_{\text{element}}$  was calculated from

$$\delta M_{\text{element}} = \left[ \frac{M_{\text{element}}}{M_{\text{Zn}}} \Big|_{\text{exp.}} - \frac{M_{\text{element}}}{M_{\text{Zn}}} \Big|_{\text{cert.}} \right] / \frac{M_{\text{element}}}{M_{\text{Zn}}} \Big|_{\text{cert.}}$$

with  $M_{\text{element}} = \sum_i m_{\text{element } i}$

(1)

where  $M_{\text{element}}/M_{\text{Zn}}|_{\text{exp.}}$  refers to the experimental mass ratio, and  $M_{\text{element}}/M_{\text{Zn}}|_{\text{cert.}}$  to the certified value. The index  $i$  denotes the overall number of impactor stages. In Fig. 9, the size dependence of  $\delta M_{\text{element}}$  referred to as  $\delta m_{\text{element}, i}$  is graphically shown for Ca, Sr, Ba, and Pb (see Fig. 9 caption). Please note that the size-dependent deviation  $\delta m_{\text{element}, i}$  has been calculated setting  $\sum_i \delta m_{\text{element}, i} = 0$ . Therefore, the zero

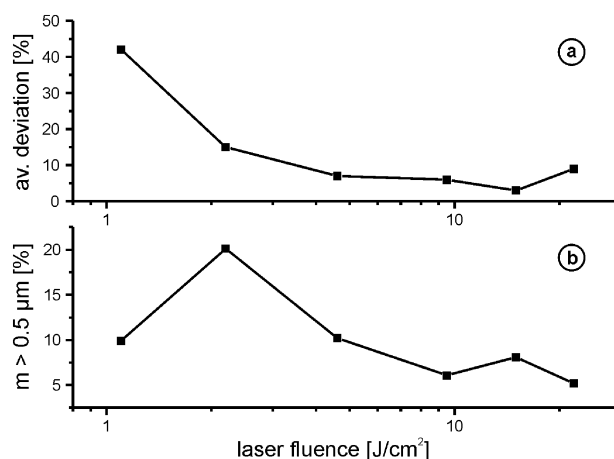


**Fig. 8** The relative percentage of particles (aerosol mass) beyond a particle diameter of  $0.5 \mu\text{m}$  plotted *vs.* the fluence applied.

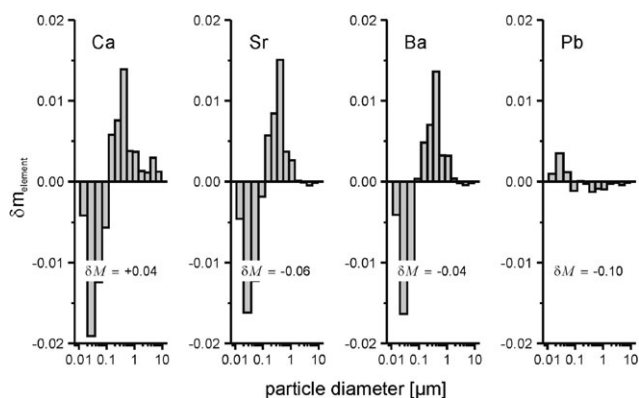


**Fig. 9** Typical deviation of the elemental mass ratio for NIR-fs-LA of silicate glass performed at a fluence of  $9.5 \text{ J cm}^{-2}$  using Zn as internal reference. Please note that the zero line refers to the aerosol composition.  $\delta M$  indicates the total deviation of aerosol composition and corresponding bulk ratio according to the values listed in Table 1.

line indicates the actual aerosol composition. Total deviations from the certified elemental ratios  $\delta M_{\text{element}}$  are given as numbers in the lower part of Fig. 9. As can be seen, the deviations for Ba, Sr, and Pb are of the order 5 up to 10%. It has also been observed that these values marginally improve to less than 2% for increasing fluences. Taking into account a total experimental uncertainty of about 10%, these results imply an acceptable agreement between the Ba-, Sr-, and Pb-specific composition of laser-produced aerosol and bulk material, respectively.

Compared to this, the Ca-specific value showed a stronger deviation of more than 20% below  $5 \text{ J cm}^{-2}$  which continuously decreases for increasing fluences. As a consequence, the average fractionation index—defined as the arithmetic mean from all  $|\delta M_{\text{element}}|$  considered—which is shown in Fig. 8(a) has been found to converge towards a level of less than 10% for fluences beyond  $5 \text{ J cm}^{-2}$ . The origin of the Ca-specific deviation for fluences smaller than  $5 \text{ J cm}^{-2}$  is unclear particularly because the corresponding TXRF responses have been systematically corrected for the relevant interference, namely  $K_{\beta}$  line of potassium. Therefore, residual fractionation during the ablation process as well as non-stoichiometric aerosol formation with respect to Ca cannot completely be excluded.

## Conclusion

The elemental fractionation of dielectric aerosols produced by NIR-fs-LA of glass has been studied. Our results indicate that the Ca-, Zn-, Sr-, Ba-, and Pb-specific stoichiometry of these aerosols reflects the bulk composition if the fluence is chosen to be well above  $5 \text{ J cm}^{-2}$ . The composition of different aerosol fractions has been found to be size-dependent. Using Zn as internal standard it could be shown that particles larger than about 100 nm tend to accumulate less volatile compounds namely Ca, Sr, and Ba. In contrast, particles smaller than 100 nm were generally Zn-enriched. The Pb-specific results, however, contradict this finding since the corresponding Pb/Zn ratios have been found to follow the opposite trend, *i.e.* particles were Pb-enriched below a size of about 100 nm and depleted above. The origin of this reversal is unknown yet.

It has furthermore been demonstrated that aerosols produced by NIR-fs-LA of silicate glasses mainly consist of particles within the mesoscopic size range, *i.e.* roughly in between 10 and 100 nm. Apparently, such aerosols experience

minor losses due to diffusion or inertial forces and can therefore efficiently be transported over larger distances.

Scanning electron microscopy of impacted brass particles revealed the existence of fractal-like agglomerates which were composed of primary nanoparticles. The morphology of these deposits appears to be self-affine as a result of fractal growth during impaction. According to the hydrodynamic properties of fractal objects both single particles and corresponding agglomerates of arbitrary size may, in principle, be deposited in the same stage. It is, however, unclear whether objects whose size even exceeds several micrometers can be formed during the ablation process or transport period. Most intuitively, clustering of smaller agglomerates and single particles at the surface or right before impaction are the most likely mechanisms for creating these micrometer-sized deposits. From an analytical point of view, the formation of fractal-like agglomerates generally proves favourable as it reduces potential diffusion losses.

Taking into account results previously published on the classification of brass aerosols<sup>14</sup> it is obvious that NIR-fs-LA enables the accomplishment of stoichiometric sampling of both metallic and dielectric material if the fluence is properly chosen. According to our investigations, fs-LA of opaque glasses produces stoichiometric aerosols in a fluence range  $>5 \text{ J cm}^{-2}$  while for metals a value of about  $5 \text{ J cm}^{-2}$  should not be exceeded due to the occurrence of elemental fractionation and intensified production of micrometer particles. These fluence ranges, however, should not be taken as benchmark values for all materials since they are supposed to vary, in particular, if UV-transparent matrices are under investigation. The latter finding moreover refers to fs-LA applying pulse durations of 200–250 fs and main to pre(post)-laser pulse intensity ratios of about  $10^2$ . Recent measurements carried out in our laboratory have shown that stoichiometric sampling of brass can even be realized for fluences up to  $50 \text{ J cm}^{-2}$  if shorter pulses ( $<150 \text{ fs}$  duration) with an improved pre(post)-pulse intensity ratio of  $5 \times 10^3$  are used.<sup>25</sup>

## Acknowledgements

Financial support by the German Science Foundation (Deutsche Forschungsgemeinschaft/Project KO 2274/2)<sup>26</sup> is gratefully acknowledged. Furthermore, the authors thank Mrs Meuris from the Centre of Electron Microscopy (ZENN) at the University of Dortmund (Germany) and Dr C. Van Gulijk from the University of Delft (Netherlands) for providing SEM micrographs of brass and soot particles, respectively. The remarks made by both referees were very helpful to improve the quality of the manuscript and are also gratefully acknowledged.

## References

- 1 A. L. Gray, *Analyst*, 1985, **110**, 551.
- 2 P. Arrowsmith, *Anal. Chem.*, 1987, **59**, 1437.
- 3 R. E. Russo, X. L. Mao, O. V. Borisov and H. C. Liu, *J. Anal. At. Spectrom.*, 2000, **15**, 1115.
- 4 D. Bleiner and D. Günther, *J. Anal. At. Spectrom.*, 2001, **16**, 449.
- 5 A. M. Leach and G. M. Hieftje, *Appl. Spectrosc.*, 2002, **56**, 62.
- 6 X. Mao and R. E. Russo, *J. Anal. At. Spectrom.*, 1997, **12**, 177.
- 7 C. Pickhardt, J. S. Becker and H. -J. Dietze, *Fresenius J. Anal. Chem.*, 2000, **368**, 173.
- 8 M. D. Norman, W. L. Griffin, N. J. Pearson, M. O. Garcia and S. Y. O'Reilly, *J. Anal. At. Spectrom.*, 1998, **13**, 477.
- 9 S. Gao, X. M. Liu, H. L. Yuan, B. Hattendorf, D. Günther, L. Chen and S. H. Hu, *Geostand. Newsl.*, 2002, **26**, 181.
- 10 K. Niemax, *Fresenius J. Anal. Chem.*, 2001, **370**, 332.
- 11 B. N. Chichkov, C. Momma, S. Nolte, F. von Alvensleben and A. Tünnermann, *Appl. Phys. A*, 1996, **63**, 109.
- 12 R. E. Russo, X. Mao, J. J. Gonzalez and S. S. Mao, *J. Anal. At. Spectrom.*, 2002, **17**, 1072.

§ Please note that in the present paper the term "fractionation" refers to deviations of the aerosol composition from the actual bulk value rather than the time dependence of relative elemental responses as defined by Fryer *et al.*<sup>24</sup>

- 
- 13 Q. Z. Bian, J. Koch, H. Lindner, H. Brandt, R. Hergenröder and K. Niemax, *J. Anal. At. Spectrom.*, 2005, DOI: 10.1039/b500632e.
  - 14 J. Koch, A. von Bohlen, R. Hergenröder and K. Niemax, *J. Anal. At. Spectrom.*, 2004, **19**, 267.
  - 15 H. Varel, PhD thesis, Free University of Berlin, 1999.
  - 16 M. Marjamäki, J. Keskinen, D. R. Chen and D. Y. H. Pui, *J. Aerosol Sci.*, 2000, **31**, 249.
  - 17 C. Van Gulijk, J. C. M. Marijnissen, M. Makkee, J. A. Moulijn and A. Schmidt-Ott, *J. Aerosol Sci.*, 2004, **35**, 633.
  - 18 A. A. Lushnikov, A. V. Pakhomov and G. A. Chernyaeva, *Sov. Phys. Dokl.*, 1987, **32**, 45.
  - 19 R. J. Samson, G. W. Mulholland and J. W. Gentry, *Langmuir*, 1987, **3**, 272.
  - 20 R. C. Flagan, *Aerosol Measurements: Principles, Techniques and Applications*, John Wiley, New York, 2001.
  - 21 L. B. Kiss, J. Soderlund, G. A. Niklasson and C. G. Granqvist, *Nanostruct. Mater.*, 1999, **12**, 327.
  - 22 B. S. Luk'yanchuk, W. Marine and S. I. Anisimov, *Laser Phys.*, 1998, **8**, 291.
  - 23 H. R. Kuhn, M. Guillong and D. Günther, *Anal. Bioanal. Chem.*, 2004, **378**, 1069.
  - 24 B. J. Fryer, S. E. Jackson and H. P. Longerich, *Can. Mineral.*, 1995, **33**, 303.
  - 25 H. Lindner, Diploma thesis, University of Dortmund, Germany, 2004.
  - 26 <http://www.dfg.de/gepris/>.